

# Inhibitor-based validation of a homology model of the active-site of tripeptidyl peptidase II

Hans De Winter\*, Henry Breslin, Tamara Miskowski,  
Robert Kavash, Marijke Somers

*Johnson and Johnson Pharmaceutical Research and Development, Turnhoutseweg 30, B-2340 Beerse, Belgium*

Received 6 September 2004; received in revised form 30 November 2004; accepted 30 November 2004

Available online 7 January 2005

## Abstract

A homology model of the active site region of tripeptidyl peptidase II (TPP II) was constructed based on the crystal structures of four subtilisin-like templates. The resulting model was subsequently validated by judging expectations of the model versus observed activities for a broad set of prepared TPP II inhibitors. The structure–activity relationships observed for the prepared TPP II inhibitors correlated nicely with the structural details of the TPP II active site model, supporting the validity of this model and its usefulness for structure-based drug design and pharmacophore searching experiments.

© 2004 Elsevier Inc. All rights reserved.

**Keywords:** Homology modeling; Structure-based drug design; Butabindide; Obesity; TPP II; Active site; Inhibitors.

## 1. Introduction

Obesity is viewed as a serious concern within our medical community because it has been correlated with a number of undesirable diseases and disorders, including diabetes, hypertension, gall bladder disease, and osteoarthritis [1]. New therapeutic agents addressing the obesity problem could help offset the morbidity and physically and economically draining diseases, while concurrently yielding yearly revenues in the billions of dollars for the marketers of such products. A number of new strategies are currently being explored to address the obesity problem, as described in many comprehensive reviews of past and present approaches [2–5]. Among the many approaches being explored is the evaluation of various satiety enhancing agents. One reported endogenous satiety agent is the octapeptide cholecystokinin (CCK-8, DYMGWMDF-NH<sub>2</sub>), which has demonstrated significant in vivo inhibitory feeding effects. Some researchers have attempted to exploit this desired effect of CCK-8 by preparing non-peptidyl

analogs of CCK-8, and these compounds are currently at various stages of development.

Instead of CCK-8 mimics, an alternate approach recently reported was based towards enhancing CCK-8's natural response by inhibiting CCK-8's normal degradation [6]. CCK-8 is degraded biochemically by a membrane-bound isoform of tripeptidyl peptidase II (TPP-II; EC 3.4.14.10), whose function was not previously known. The serine peptidase is found in neurons that responded to CCK-8 as well in nonneuronal cells. It inactivates CCK-8 in two steps that correspond to CCK-5 (GWMDF-NH<sub>2</sub>) and GWM. Both fragments are biologically inactive. The discovery of tripeptidyl peptidase II in rat liver cytosol was first reported in 1983 and the enzyme has been extensively characterized since then [6–9]. It is an extralysosomal serine peptidase with an active site of the subtilisin type. TPP II is built up of 138 kDa subunits forming a well-organized oligomeric structure with a native molecular weight of more than 10<sup>3</sup> kDa [10]. Inhibitors of the peptidase have been designed in a rational manner resulting in the discovery of UCL-1371 [6] (Fig. 1, 2). This compound inhibits the CCK-inactivating peptidase with an inhibition constant of 80 nM. Based on progressive optimisation of UCL-1371, Rose et al. [6] and

\* Corresponding author. Tel.: +32 14 60 29 97; fax: +32 14 60 55 61.  
E-mail address: [hdwinter@prdbe.jnj.com](mailto:hdwinter@prdbe.jnj.com) (H. De Winter).

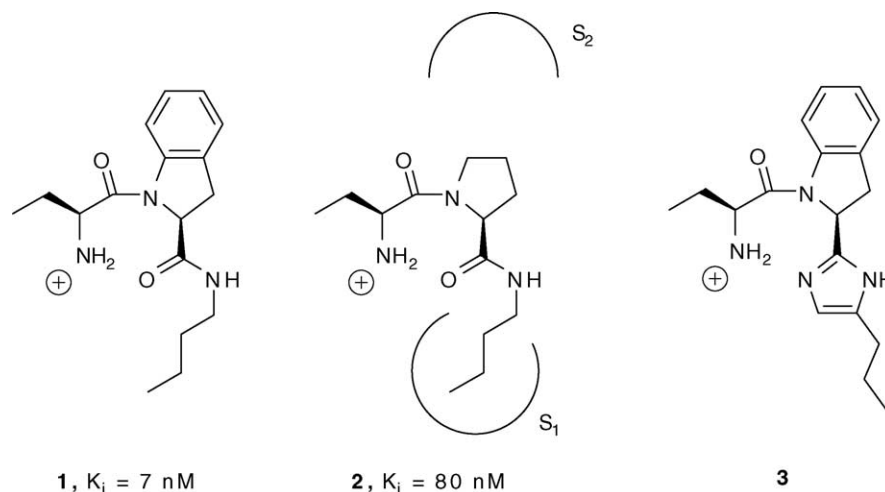


Fig. 1. Butabindide (**1**) and UCL-1371 (**2**) have been described as potent inhibitors of TPP II [6]. The proposed binding mode of **2** within the active site of TPP II is indicated. Compound **3** is a close analogue of butabindide and about twice as active [12].

Rose and co workers [11] arrived at an indoline analogue (UCL-1397, butabindide, **1**) with an inhibition constant of 7 nM. When **1** was administered intravenously to starved mice, a significant satiating effect was observed that was selectively blocked by devazepide, a CCK-A receptor antagonist. Butabindide was also shown to significantly reduce food intake in rats.

In our own research laboratories, early lead-optimisation efforts has driven the synthesis of analogues of butabindide, in which the butylamide sidechain has been replaced by imidazole moieties [12,13]. The most active compound within this series has an  $IC_{50}$  of 4 nM (Fig. 1, **3**), and is furthermore less prone to degradation when compared to butabindide [12,13].

The enzyme tripeptidyl peptidase II is a cytosolic peptidase showing reasonable sequence homology with subtilisin, despite the fact that TPP II constitutes about 1250 amino acids and subtilisin only 275 [14,15]. Fig. 2 provides a schematic overview of the sequence alignment between these two enzymes. Since TPP II is about 975 residues longer in length compared to subtilisin, there are a number of loop regions within the sequence of TPP II that do not have any similarity with the subtilisin protein. These loops are indicated by yellow boxes in Fig. 2 and are labeled L1–L3. These loops are separating regions of high similarity between both proteins, which include the active site region and in particular the catalytically crucial Asp-His-Ser triads. The sequence similarity between the overlapping parts of

both enzymes (excluding the loop regions of TPP II) is around 30%, sufficient to justify the use of the subtilisin crystal structure as a template for building a homology model of the active site region of TPP II.

In this paper, we describe the building of an homology model of the active-site region of TPP II, and the subsequent validation of this model by means of a number of established structure–activity relationships and docking techniques based on close analogues of **3** [12,13].

## 2. Methodology

### 2.1. Homology modeling

#### 2.1.1. Template structures

The program BLAST was used to search the Brookhaven Protein Databank (PDB) [16] protein structure database for structures having high sequence similarity for TPP II. Four structures were retrieved as templates based on their sequence similarity with TPP II. Details of these structures are listed in Table 1, cross-similarities are provided in Table 2, and the sequence alignment is visualized in Fig. 3.

#### 2.1.2. Sequence alignment

Due to the many loops in the sequence of TPP II as compared to subtilisin and similars (Figs. 2 and 3), and also due to the fact that the primary objective of building a TPP

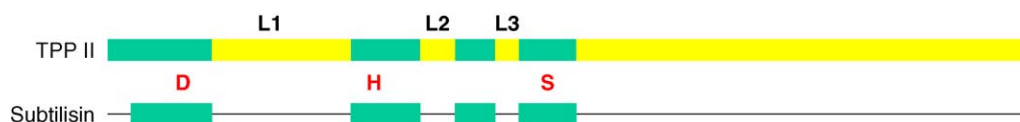


Fig. 2. Schematic overview of the sequence alignment between TPP II and subtilisin. Green boxes represent regions of similarity; yellow boxes are additional loops within the TPP II sequence for which there is no sequence overlap with subtilisin. Also indicated are the approximate positions of the three catalytical residues Asp (D), His (H), and Ser (S) along both sequences. The immediate environments of these residues are quite similar between the two sequences. (For interpretation of the references to colour in this figure legend, the reader is referred to the web version of the article.)

Table 1

Summary of the crystal structures that served as templates to build the TPP II model

PDB code	Name	Reference	Classification	Resolution (Å)	Source
1SCA	Subtilisin	[17]	E.C. 3.4.21.62	2.0	<i>Bacillus licheniformis</i>
2ST1	Subtilisin	[18]	E.C. 3.4.21.62	1.8	<i>Bacillus amyloliquefaciens</i>
3TEC	Thermitase	[19]	E.C. 3.4.21.14	2.0	<i>Thermoactinomyces vulgaris</i>
2PKC	Proteinase K	[20]	E.C. 3.4.21.64	1.5	<i>Tritirachium album</i>

II model was to support the in-house chemistry programs aimed at discovering potent inhibitors, the strategy was adopted to focus only on the active site region of TPP II and not to model the loop regions. As such, the sequences Met<sub>1</sub>-Leu<sub>25</sub> (amino-terminal part), Thr<sub>57</sub>-Val<sub>258</sub> (Loop 1), Val<sub>369</sub>-Pro<sub>389</sub> (Loop 2), Thr<sub>408</sub>-Thr<sub>442</sub> (Loop 3), and the entire carboxy-terminal part starting from His<sub>499</sub> have not been

modeled. An alternative approach, in which these loops are replaced with six to seven glycine residues followed by energy minimization, has not been performed [21–26].

### 2.1.3. Model building

A model of TPP II was calculated using the homology modeling program Modeller version 5 [27] and was based on

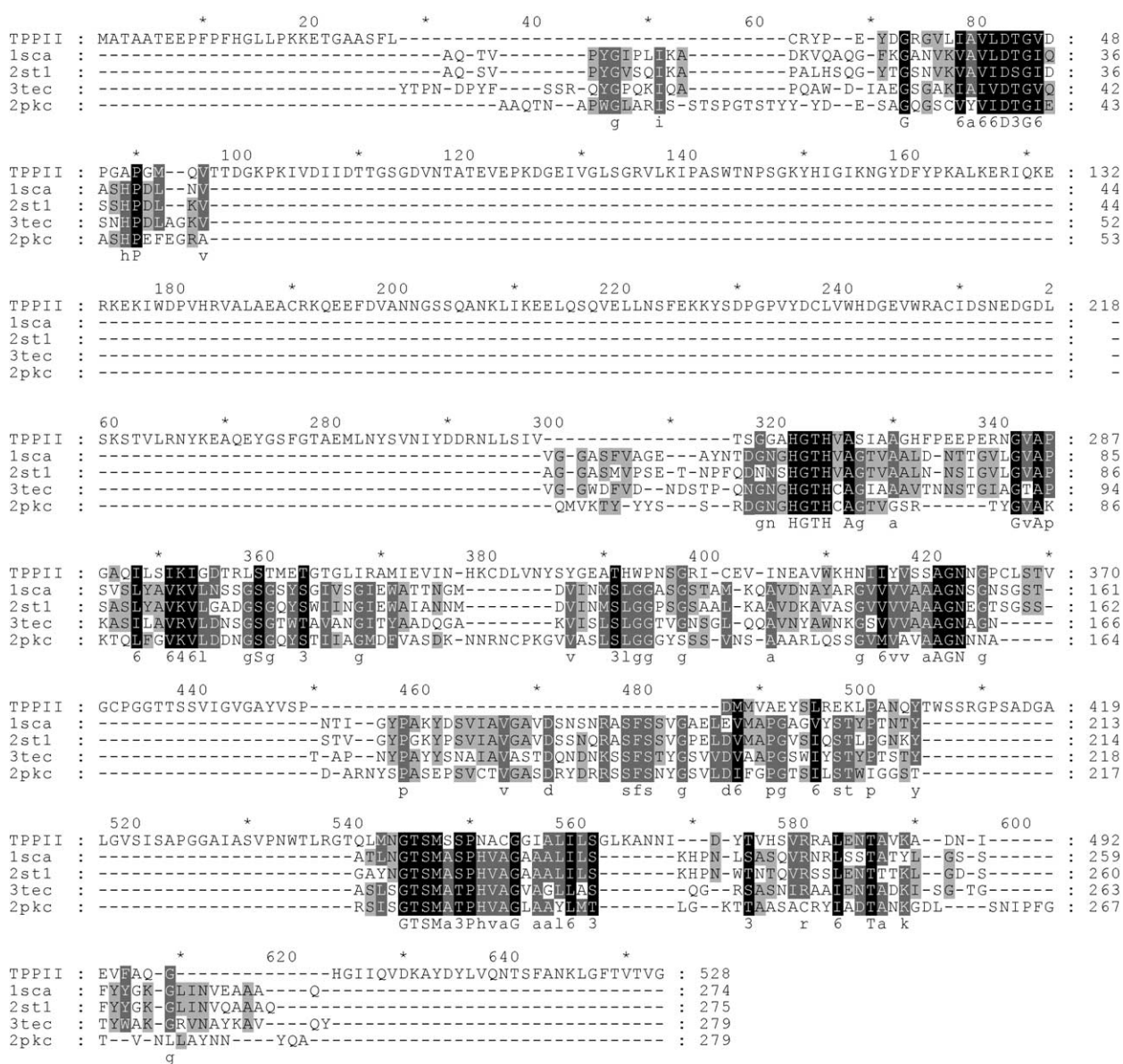


Fig. 3. Sequence alignment between TPP II and the four template crystal structures. Only the first 528 residues starting at the amino-terminus of TPP II are shown. Alignment of the four template structures is based on superimposition of their three-dimensional conformations.

Table 2

Cross-identities (upper-right part) and similarities (lower-left part) between the four crystal structures that have been used as a template for homology modeling, and the TPP II sequence

	TPPII	1SCA	2ST1	3TEC	2PKC
TPPII	1.00	0.19	0.21	0.18	0.13
1SCA	0.30	<i>1.00</i>	<i>0.69</i>	<i>0.43</i>	<i>0.28</i>
2ST1	0.31	<i>0.79</i>	<i>1.00</i>	<i>0.39</i>	<i>0.29</i>
3TEC	0.27	<i>0.62</i>	<i>0.54</i>	<i>1.00</i>	<i>0.26</i>
2PKC	0.23	<i>0.42</i>	<i>0.41</i>	<i>0.42</i>	<i>1.00</i>

The values between the four template structures have been calculated from structural alignments (indicated in italics).

the sequence alignment as shown in Fig. 3. Default parameters were used. No ligand was present in the active site of TPP II whilst calculating the structure. Because the final result is only a model of the active site region of the protein lacking large bridging loops, attempts to further refine the model by means of energy minimisation and/or molecular dynamics calculations were not performed.

## 2.2. Docking

Hydrogens were added to the protein at standard positions, and all acid and basic residues were carefully inspected to check for their most-likely protonation states based on the analysis of their immediate residue surroundings. Subsequently, the program Gold [28] was used to dock all small molecule compounds into the active site of TPP II. Default docking parameters were applied.

The program GRID [29], version 1.6, was used to validate the results obtained from docking and to analyse the active site in terms of interaction points. This was done using a grid-size of  $1/3 \text{ \AA}$ , and a box-size covering the entire active site region with an extend of  $5.0 \text{ \AA}$ .

## 2.3. Chemistry and biochemistry

Related synthesis for actual TPP II inhibitors reported within, as well as biochemical techniques used to measure

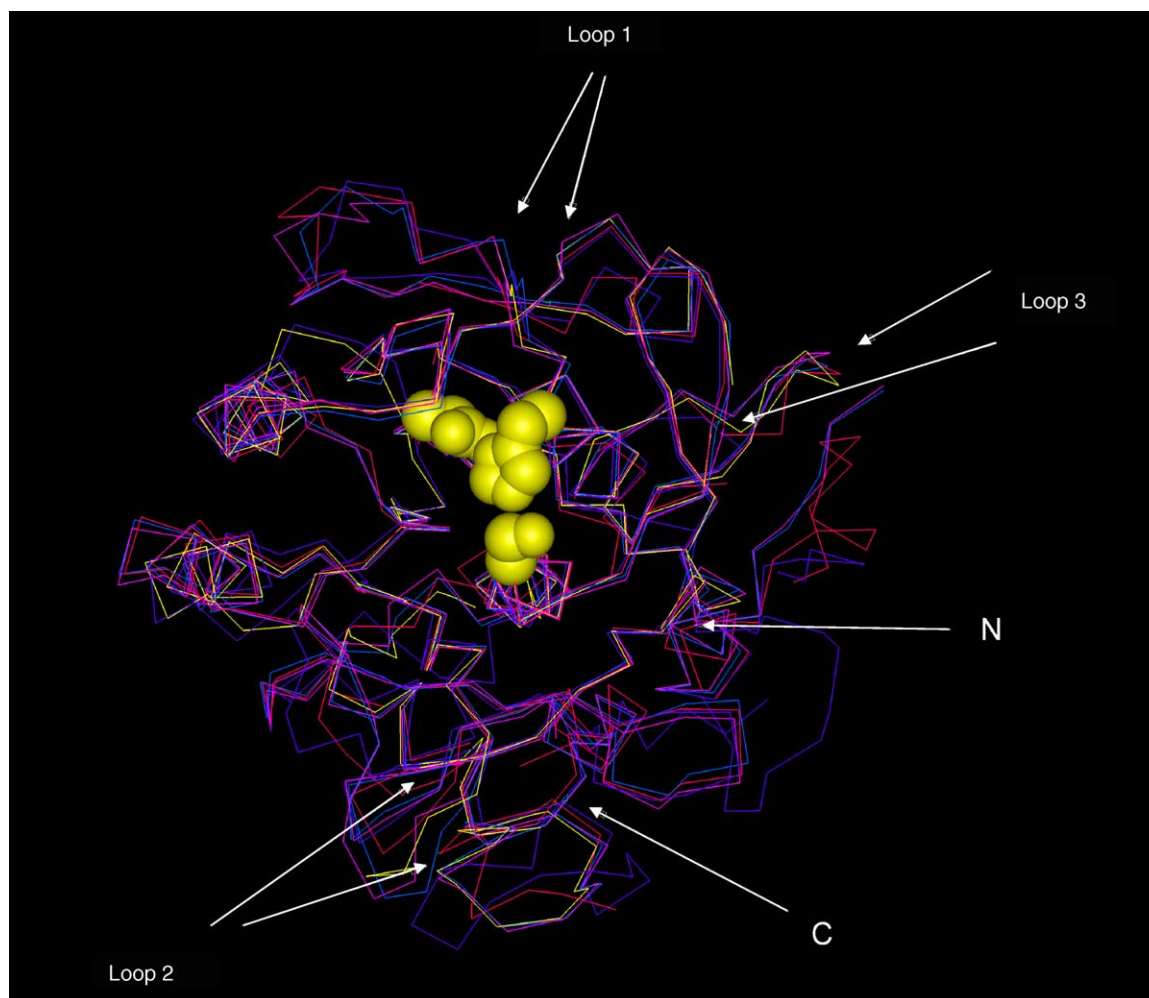


Fig. 4. Ribbon representation of the TPP II model (yellow) superimposed onto the four reference structures (3TEC, orange; 2ST1, pink; 2PKC, purple; 1SCA, dark cyan). CPK models of the three catalytically important residues Asp, His, and Ser in the active of TPP II are shown in yellow. The positions of the loops that have not been modeled (loops 1–3), together with the N- and C-termina, are indicated by arrows. (For interpretation of the references to colour in this figure legend, the reader is referred to the web version of the article.)



related biological activities have been described in our earlier reports [12,13].

### 3. Results and discussion

#### 3.1. The homology model

A ribbon presentation of the model superimposed onto the structures of the four protein templates is shown in Fig. 4. From this figure it is clear that the regions where the loops are sprouting from the model are located at the surface, and are also a relatively long distance separated from the actual active site region. This provides some support to the original assumption that omitting these regions from the model should not have a drastic influence on the conformations of the active site region residues.

#### 3.2. Docking of butabindide and its close analogue 3

Following the construction of the TPP II model, the nanomolar inhibitors butabindide, **1**, and its close analogue **3**, were docked in the active site. Both molecules fit into the active site quite nicely, adopting conformations that are very close to their global minimum energy

conformations. Interestingly, only the (*S*)-configurations of both molecules fit in this pocket (Fig. 5a and b). This is consistent with the observation that the (*R*)-configuration of compound **4** is inactive up to a concentration of >10,000 nM (Table 3), clearly demonstrating the enzymatic stereospecificity requirement for good inhibitors of TPP II.

All functional heteroatoms of the butabindide inhibitor are within hydrogen bonding distance of the protein residues (Fig. 5c). The basic primary aminogroup of butabindide forms hydrogen bonds with both Asp<sub>43</sub> (O...N distance  $\sim 3.7$  Å) and with the backbone oxygen of Thr<sub>333</sub> (O...N distance  $\sim 2.9$  Å). Although the O of the butylamide sidechain is not involved in any obvious interactions with the protein, it is located within hydrogen bonding distance ( $\sim 3.0$  Å) of the basic amino group of butabindide, forming as such an intramolecular interaction which is stabilizing the bound conformation. Thr<sub>303</sub> is donating a hydrogen bond to the tertiary amide O of butabindide (O...O  $\sim 2.8$  Å), while the butylamide nitrogen is forming a hydrogen bond with the backbone O of Trp<sub>335</sub> (N...O  $\sim 3.5$  Å). In the case of analogue **3**, the imidazole N is forming a similar hydrogen bond with Trp<sub>335</sub>.

A number of hydrophobic interactions between the inhibitor and the protein can also be identified (Fig. 5c).

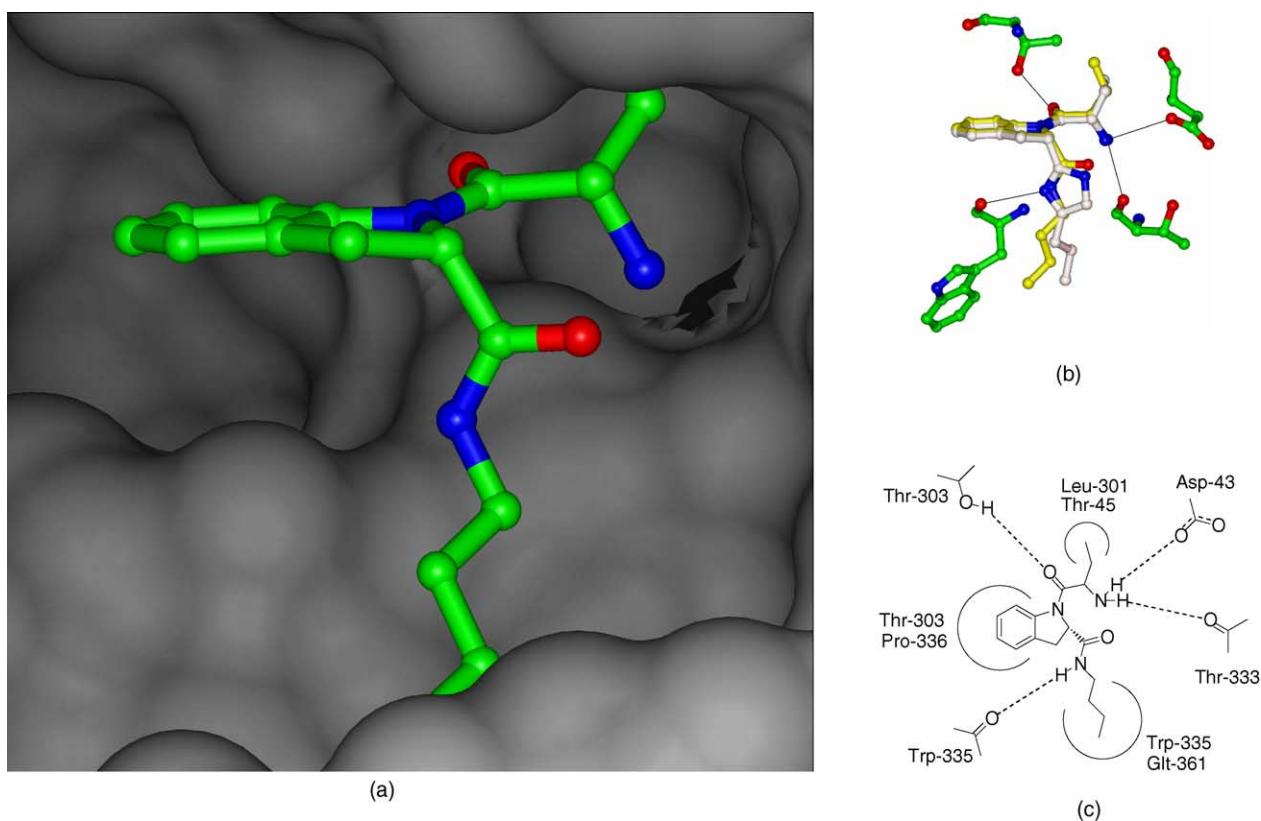
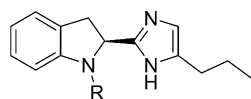


Fig. 5. The putative binding modes of butabindide and **3** into the active site model of TPP II. (a) Global view into the pocket. Butabindide is shown in ball-and-stick representation, with atoms colored according to their type. (b) Overlap of butabindide (yellow) with the imidazole analogue **3** (white). (c) Analysis of the binding interactions as exemplified for butabindide. (For interpretation of the references to colour in this figure legend, the reader is referred to the web version of the article.)

Table 3

Explored structure–activity relations for a number of chemical modifications along segment A



Number	R	IC <sub>50</sub> (nM)
3		4
7		22
8		40 (racemic)
9		20
10		4
11		2300

The planar phenyl ring is nicely located in a groove of the active site flanked by Thr<sub>303</sub> and Pro<sub>336</sub>. In addition, the butylchain of butabindide, and the corresponding propyl chain in **3**, fit nicely into the deep and hydrophobic S1-pocket formed by Trp<sub>335</sub> and Gly<sub>361</sub>. Interestingly, it has been speculated that this S1-pocket is involved in occupying the large hydrophobic sidechain of the Met<sub>3</sub> residue of the CCK-8 natural substrate [6]. Finally, as an example of a third hydrophobic interaction, the ethyl sidechains of both inhibitors fit nicely into a small pocket formed by the sidechains of Leu<sub>301</sub> and Thr<sub>45</sub>.

### 3.3. GRID analysis of the active site

GRID-based interaction energy calculations sometimes yield useful information on the likeliness of a putative binding mode, and sometimes also provide useful clues regarding additional interaction points within the binding pocket under investigation [29]. In this respect, a GRID calculation was performed using a number of interaction probes, including a methyl-probe to model hydrophobic interactions, and an amide NH<sub>2</sub>-probe to mimic hydrogen bond donor interactions. Fig. 6 summarizes visually the results for these two probes.

#### 3.3.1. Methyl-probe

Focussing in first instance on the methyl-probe to investigate hydrophobic interactions, there is a nice overlap between the calculated interaction contours and the predicted locations of the aromatic, butyl, and ethyl sidechains of **3** (Fig. 6, green contours). Especially the agreement between the contours and the location of the ethyl sidechain, which is positioned in a small pocket flanked by residues Leu<sub>301</sub> and Thr<sub>45</sub>, is quite convincing. The contouring of the methyl-probe energies also indicates that is probably not possible to allocate larger sidechains into this small pocket. On the other hand, the propylimidazole sidechain is located into the large hydrophobic S1-pocket, and in this region there is also a nice overlap apparant with the calculated energy contours for the methyl-probe. This indicates that the S1-pocket is a rather hydrophobic area in which a propyl-like sidechain likes to reside. Finally, behind the aromatic ring of compound **3** there is also a region of significant attractive interaction for a methyl-probe. This region, which is not occupied by **3** nor by butabindide, offers interesting opportunities for improved inhibitor design.

#### 3.3.2. Amide NH<sub>2</sub> probe

As a prototype of a hydrogen bond donating functionality, the amide probe seems to reside preferentially in the regions that coincide with the locations of the primary amine N and the O of the tertiary amide of compound **3** (Fig. 6, blue contours). Again, this provides firm support for the proposed binding mode, in which the primary amine N is making hydrogen bonds with both Asp<sub>43</sub> and Thr<sub>333</sub>, and where the O of the tertiary amide is hydrogen bonded to Thr<sub>303</sub>.

### 3.4. Inhibitor-based model validation

In a second stage, information from a number of chemical variations of **3** with their the corresponding activity profiles was used to validate both the working model of TPP II and the proposed mode of binding of butabindide-derived inhibitors. In this respect, compound **3** was logically divided into three different segments (Fig. 7), and each of these segments were subjected to small chemical variations in order to explore the underlying structure–activity relationships.

#### 3.4.1. Segment A

(a) The ethyl groups of both butabindide and **3** are located in the same hydrophobic pocket flanked by residues Leu<sub>301</sub> and Thr<sub>45</sub>. According to the TPP II subtilisin homology model and to the GRID-based analysis, this region can occupy only small hydrophobic moieties such as methyl, ethyl or propyl groups. If this hypothesis is valid, one should expect that compounds having significantly larger hydrophobic substituent along this segment of the molecule should be less active as compared to butabindide and compound **3**. Table 3 summarizes the structure–activity relations for a number

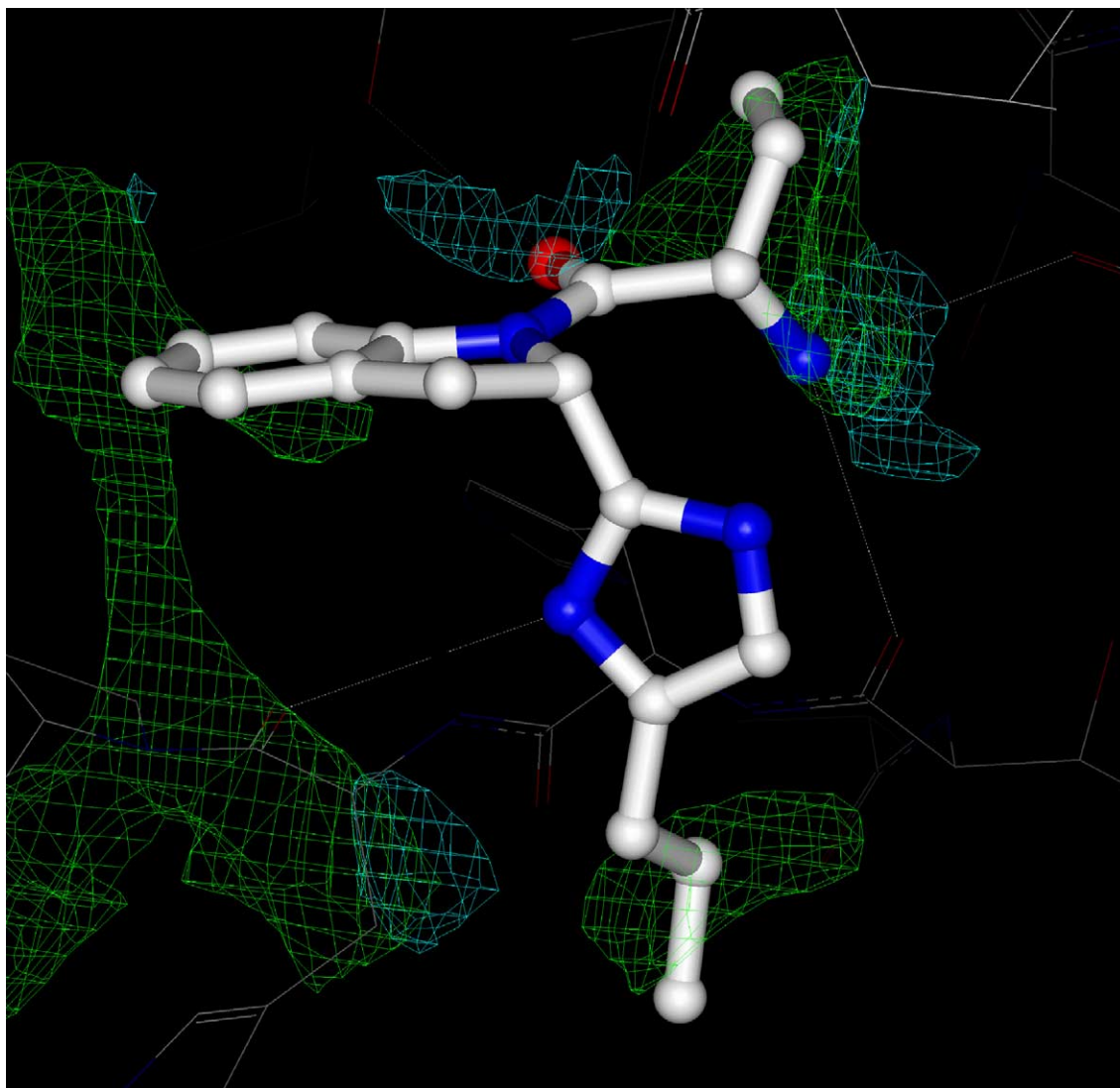


Fig. 6. Results from GRID calculations on the active site of the TPP II model. During the calculations, the inhibitor was removed from the active site. Blue lines are the interaction energy contours for an amide  $\text{NH}_2$  probe contoured at  $-10$  kcal/mol. Green lines are for a methyl probe contoured at  $-3$  kcal/mol. Compound **3**, colored with white C atoms, is shown as reference. (For interpretation of the references to colour in this figure legend, the reader is referred to the web version of the article.)

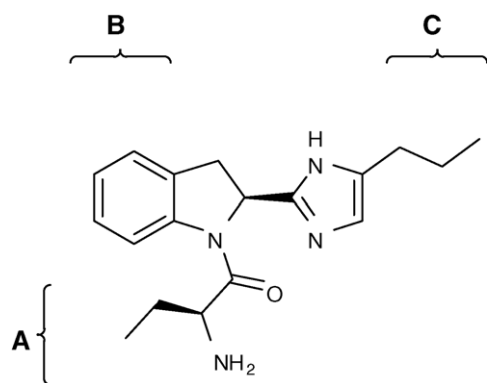


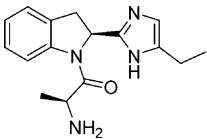
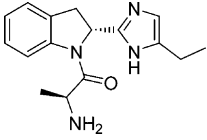
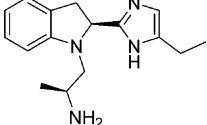
Fig. 7. Separation of compound **3** into small segments to explore the SAR and validity of the TPP II model.

of molecules that have been chemically modified along segment A. As expected from this model, the most active compounds in this series are those having small hydrophobic functionalities along this side, with a propyl or ethyl group being the best choice. Slightly less active (i.e.  $\text{IC}_{50} \sim 20$  nM) are those molecule having smaller (examples **7** and **8**) or somewhat bulkier substituents (example **9**). Much larger groups, like a benzyl group, clearly do not fit well into the pocket as reflected by the lack of activity of **11**.

- (b) According to the proposed binding model, the carbonyl functionality of butabindide is accepting a hydrogen bond from the hydroxyl group of Thr<sub>303</sub>. Therefore, replacement of this carbonyl by a methylene should lead

Table 4

Structure–activity relations with respect to the required chirality and the carbonyl moiety along segment A

Number	R	IC <sub>50</sub> (nM)
4		22
5		>10,000
6		>10,000

to a drastic drop in activity, and this is found to hold true experimentally (Table 4, compound 6 relative to 4).

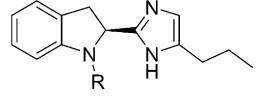
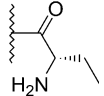
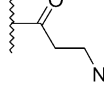
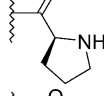
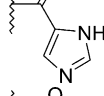
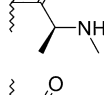
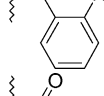
- (c) The positively-charged primary amino functionality of butabindide forms a salt-bridge to the catalytically-important Asp<sub>43</sub>, and is also hydrogen-bonded to Thr<sub>333</sub>. In fact, according to the calculated model of TPP II, this charged moiety fits nicely into the active site and it seems that replacing this group with alternative functions could rather be detrimental for activity. This modeling hypothesis is in agreement with observed experimental results, as shown in Table 5 where the SAR for a number of amino group replacements are listed. None of the listed amino modifications are successful; most, if not all, modifications lead to compounds devoid of any activity at 10  $\mu$ M concentrations, with the sole exception of compound 13 with an IC<sub>50</sub> of 1.4  $\mu$ M. These data support the hypothesis that a primary basic center is required for activity.

### 3.4.2. Segment B

According to the GRID analysis of the TPP II active site, there are interesting opportunities to substitute small hydrophobic substituents at the 4-position of the phenyl ring of butabindide (Fig. 6). In this respect, a number of phenyl substitutions were prepared and the resulting structure–activity results are summarized in Table 6. From all evaluated molecules, the 4-chloro compound 19 is about four times more potent than the reference 8, while the somewhat larger methoxy substitution 20 gives a slight decrease in activity. The 4-fold increase in activity as observed for 19 is somewhat less pronounced when extrapolated to the enantiomeric pure counterparts: a 1.3-fold increase when transforming compound 3 into its 4-chloro derivative, and about 1.2- and 2-fold increases in potency for the chloro-derivatives of 7 and 4, respectively (data not shown).

Table 5

Explored structure–activity relations for a number of chemical modifications of the amino function along segment A

Number	R	IC <sub>50</sub> (nM)
3		4
12		>10,000
13		1400
14		>10,000
15		>10,000
16		>10,000
17		>10,000

### 3.4.3. Segment C

The substituted imidazole ring of 3 can be modeled to bind into the S1-pocket of the active site. According to the TPP II model, and also supported by the favorable interaction energies for a methyl-probe in this particular region, this S1-pocket is quite hydrophobic and large enough to accept butyl-sized side-chains. In this respect, one could

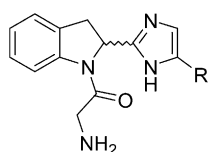
Table 6


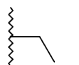
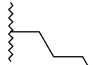
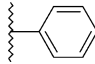
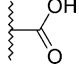
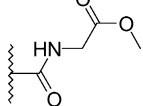
Structure–activity relations with respect to segment B

Number	R	IC <sub>50</sub> (nM)
8	–H	40
18	–F	46
19	–Cl	11
20	–OMe	67



Table 7  
Explored structure–activity relations for a number of chemical modifications along segment C



Number	R	IC <sub>50</sub> (nM)
8		40
21		194
22		50
23		≥10,000
24		>10,000
25		4300

except that more polar, but also smaller and bulkier side-chains, will give less optimal activities. This hypothesis has been challenged by a number of chemical variations, which are summarized in Table 7. Not surprisingly, the highest potency is found for the propyl compound **8**, while smaller (**21**) and larger (**22**) substitutions all lead to decreased activities. On the extreme side of this spectrum, phenyl substitutions, which are much bulkier compared to butyl side-chains, are even devoid of any activity (**23**). Finally, polar substitutions, like in **24** and **25**, are found to be inactive as well.

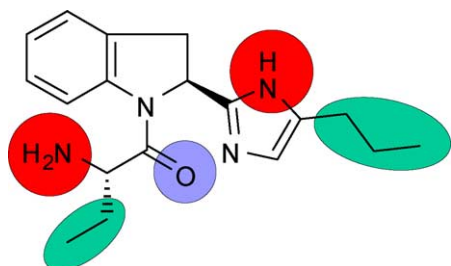


Fig. 8. Five-points pharmacophore for TPP II inhibition based on the active site model and the established structure–activity relations. Green are hydrophobic areas, red are hydrogen bond donors, and blue are hydrogen bond acceptors. (For interpretation of the references to colour in this figure legend, the reader is referred to the web version of the article.)

## 4. Conclusions

This paper describes an approach for the design of a model of the active site region of TPP II, and the subsequent validation of this model by the exploration of the structure–activity relationships for a wide range of TPP II-based inhibitors. Although the usefulness of a homology model for structure-based drug design is often limited by the fact that small variations of residue conformations within the binding region are difficult to predict, the here presented model of TPP II is nevertheless in line with the observed structure–activity relationships for a significant number of inhibitors. This has prompted us to integrate the use of this model in our internal drug discovery programs.

The here presented findings point into the direction of a minimal five-points pharmacophore model for the inhibition of TPP II (Fig. 8). These five requirements include the presence of two hydrophobic moieties, two hydrogen bond donating group, of which one should preferably be positively charged, and one hydrogen bond acceptor function.

## Acknowledgment

We appreciate the input from Prof. Dr. Jan Tollenaere.

## References

- [1] I. Wickelgren, Obesity, how big a problem? *Science* 280 (1998) 1364–1367.
- [2] J.-A. Fernandez-Lopez, X. Remesar, M. Foz, M. Alemany, Pharmacological approaches for the treatment of obesity, *Drugs* 62 (2002) 915–944.
- [3] H. Hauner, Current pharmacological approaches to the treatment of obesity, *Int. J. Obesity* 25 (2001) 102–106.
- [4] I.L. Mertens, L.F. Van Gaal, Promising new approaches to the management of obesity, *Drugs* 60 (2000) 1–9.
- [5] C.P. Kordik, A.B. Reitz, Pharmacological treatment of obesity: therapeutic strategies, *J. Med. Chem.* 42 (1999) 181–201.
- [6] C. Rose, F. Vargas, P. Facchinetti, P. Bourgeat, R.B. Bambal, P.B. Bishop, S.M.T. Chan, A.N.J. Moore, C.R. Ganellin, J.-C. Schwartz, Characterization and inhibition of a cholecystokinin-inactivating serine protease, *Nature* 380 (1996) 403–409.
- [7] R.-M. Bälöw, U. Ragnarsson, Ö. Zetterqvist, Tripeptidyl aminopeptidase in the extralysosomal fraction of rat liver, *J. Biol. Chem.* 258 (1983) 11622–11628.
- [8] B. Tomkinson, Nucleotide sequence of cDNA covering the N-terminus of human tripeptidyl peptidase II, *Biomed. Biochim. Acta* 50 (1991) 4–6.
- [9] R.-M. Bälöw, I. Eriksson, Tripeptidyl peptidase II in haemolysates and liver homogenates of various species, *Biochem. J.* 241 (1987) 75–80.
- [10] B. Tomkinson, Tripeptidyl peptidases: enzymes that count, *TIBS* 24 (1999) 355–359.
- [11] C.R. Ganellin, P.B. Bishop, R.B. Bambal, S.M.T. Chan, J.K. Law, B. Marabout, P.M. Luthra, A.N.J. Moore, O. Peschard, P. Bourgeat, C. Rose, F. Vargas, J.-C. Schwartz, Inhibitors of tripeptidyl peptidase II. 2. Generation of the first novel lead inhibitor of cholecystokinin-8-

- inactivating peptidase: a strategy for the design of peptidase inhibitors, *J. Med. Chem.* 43 (2000) 664–674.
- [12] H.J. Breslin, T.A. Miskowski, M.J. Kukla, W.H. Leister, H.L. De Winter, D.A. Gauthier, M.V.F. Somers, D.C.G. Peeters, P.W.M. Roevens, Design, synthesis, and tripeptidyl peptidase II inhibitory activity of a novel series of (S)-2,3-dihydro-2-(4-alkyl-1H-imidazol-2-yl)-1H-indoles, *J. Med. Chem.* 45 (2002) 5303–5310.
- [13] H.J. Breslin, T.A. Miskowski, M.J. Kukla, H.L. De Winter, M.V.F. Somers, P.W.M. Roevens, R.W. Kavash, Tripeptidyl-peptidase II (TPP II) inhibitory activity of (S)-2,3-dihydro-2-(1H-imidazol-2-yl)-1H-indoles, a systematic SAR evaluation. Part 2, *Bioorg. Med. Chem. Lett.* 13 (2003) 4467–4471.
- [14] B. Tomkinson, A.-K. Jonsson, Characterization of cDNA for human tripeptidyl peptidase II: the N-terminal part of the enzyme is similar to subtilisin, *Biochemistry* 30 (1991) 168–174.
- [15] B. Tomkinson, C. Wernstedt, U. Hellman, Ö. Zetterqvist, Active site of tripeptidyl peptidase II from human erythrocytes is of the subtilisin type, *Proc. Natl. Acad. Sci. U.S.A.* 84 (1987) 7508–7512.
- [16] H.M. Berman, J. Westbrook, Z. Feng, G. Gilliland, T.N. Bhat, H. Weiss, I.N. Shindyalov, P.E. Bourne, The protein data bank, *Nucleic Acids Res.* 28 (2000) 235–242.
- [17] P.A. Fitzpatrick, A.C. Steinmetz, D. Ringe, A.M. Klivanov, Enzyme crystal structure in a neat organic solvent, *Proc. Natl. Acad. Sci. U.S.A.* 90 (1993) 8653–8657.
- [18] R. Bott, M. Ultsch, A. Kossiakoff, T. Graycar, B. Katz, S. Power, The three-dimensional structure of *Bacillus amyloliquefaciens* subtilisin at 1.8 Å and an analysis of the structural consequences of peroxide inactivation, *J. Biol. Chem.* 263 (1988) 7895–7906.
- [19] P. Gros, K.H. Kalk, W.G.J. Hol, Calcium binding to thermitase. Crystallographic studies of thermitase at 0, 5, and 100 mM calcium, *J. Biol. Chem.* 266 (1991) 2953–2961.
- [20] A. Mueller, W. Hinrichs, W.M. Wolf, W. Saenger, Crystal structure of calcium-free proteinase K at 1.5 Å resolution, *J. Biol. Chem.* 269 (1994) 23108–23111.
- [21] J. Wojcik, J.P. Mornon, J. Chomilier, New efficient statistical sequence-dependent structure prediction of short to medium-sized protein loops based on an exhaustive loop classification, *J. Mol. Biol.* 289 (1999) 1469–1490.
- [22] B. Das, H. Meirovitch, Solvation parameters for predicting the structure of surface loops in proteins: transferability and entropic effects, *Proteins* 51 (2003) 470–483.
- [23] H.W.T. van Vlijmen, M. Karplus, PDB-based protein loop prediction: parameters for selection and methods for optimization, *J. Mol. Biol.* 267 (1997) 975–1001.
- [24] M.J. Dudek, H.A. Scheraga, Protein structure prediction using a combination of sequence homology and global energy minimization. I. Global energy minimization of surface loops, *J. Comput. Chem.* 11 (1990) 121–151.
- [25] T. Blundell, D. Carney, S. Gardner, F. Hayes, B. Howlin, T. Hubbard, J. Overington, D.A. Singh, B.L. Sibamda, M. Sutcliffe, Knowledge-based protein modeling and design, *Eur. J. Biochem.* 172 (1988) 513–520.
- [26] M. Das Bedamati, Solvation parameters for predicting the structure of surface loops in proteins: transferability and entropic effects, *Proteins* 51 (2003) 470–483.
- [27] A. Salî, T.L. Blundell, Comparative protein modeling by satisfaction of spatial restraints, *J. Mol. Biol.* 234 (1993) 779–815.
- [28] G. Jones, P. Willett, R.C. Glen, A.R. Leach, R. Taylor, Development and validation of a genetic algorithm for flexible docking, *J. Mol. Biol.* 267 (1997) 727–748.
- [29] P.J. Goodford, A computational procedure for determining energetically favorable binding sites on biologically important macromolecules, *J. Med. Chem.* 28 (1985) 849–857.